Metabolic Engineering 18 (2013) 78–85

Contents lists available at SciVerse ScienceDirect

Metabolic Engineering

journal homepage: www.elsevier.com/locate/ymben

# Dynamic metabolic flux analysis of plant cell wall synthesis ☆

Xuewen Chen [a,*], Ana P. Alonso [b], Yair Shachar-Hill [a]

[a] Plant Biology Department and Great Lakes Bioenergy Research Center, Michigan State University, East Lansing, MI 48824, United States
[b] Molecular Genetics Department, Ohio State University, Columbus, OH 43210, United States

ARTICLE INFO

*Article history:*
Received 25 October 2012
Received in revised form
14 March 2013
Accepted 16 April 2013
Available online 30 April 2013

*Keywords:*
Dynamic metabolic flux analysis
Plant cell wall
Sucrose invertase
Metabolic engineering
Bioenergy crops

ABSTRACT

The regulation of plant cell wall synthesis pathways remains poorly understood. This has become a bottleneck in designing bioenergy crops. The goal of this study was to analyze the regulation of plant cell wall precursor metabolism using metabolic flux analysis based on dynamic labeling experiments. Arabidopsis T87 cells were cultured heterotrophically with $^{13}C$ labeled sucrose. The time course of $^{13}C$ labeling patterns in cell wall precursors and related sugar phosphates was monitored using liquid chromatography tandem mass spectrometry until steady state labeling was reached. A kinetic model based on mass action reaction mechanisms was developed to simulate the carbon flow in the cell wall synthesis network. The kinetic parameters of the model were determined by fitting the model to the labeling time course data, cell wall composition, and synthesis rates. A metabolic control analysis was performed to predict metabolic regulations that may improve plant biomass composition for biofuel production. Our results describe the routes and rates of carbon flow from sucrose to cell wall precursors. We found that sucrose invertase is responsible for the entry of sucrose into metabolism and UDP-glucose-4-epimerase plays a dominant role in UDP-Gal synthesis in heterotrophic Aradidopsis cells under aerobic conditions. We also predicted reactions that exert strong regulatory influence over carbon flow to cell wall synthesis and its composition.



## 1. Introduction

Plant cell wall material is a major component of plant biomass that mostly consists of sugar polymers (Somerville et al., 2004). It is the most abundant sugar resource on earth and a promising feedstock for biofuel production (Pauly and Keegstra, 2010). One major bottleneck in plant biomass based biofuel production is the resistance of plant cell wall to biological, chemical or physical deconstruction (Chundawat et al., 2011). Understanding plant synthesis pathways and their regulation may lead to breakthroughs in bioenergy crop design. Current research on plant cell wall synthesis is mainly focused on understanding how cell wall precursors were assembled to polysaccharides at the gene and protein levels (Bar-Peled and O'Neill, 2011; Carpita, 2012; Keegstra and Cavalier, 2011; Martinez et al., 2009; Zhang et al., 2011). The literature indicates that plant cell wall synthesis has not yet been predictively modeled at the metabolic network level. Metabolic flux analysis (MFA) provides the necessary tools to study the patterns of carbon flow and their regulation, which underpin plant growth and development.

In MFA internal carbon fluxes through metabolic networks are obtained using isotope labeling experiments (Antoniewicz et al., 2007; Nanchen et al., 2007; Sauer et al., 1999; Schmidt et al., 1997; Wiechert and de Graaf, 1997; Wiechert et al., 1997; Wittmann, 2002; Zamboni et al., 2005, 2009). Most MFA studies in plant research are performed at both isotopic and metabolic steady state, where labeled substrates are supplied to plant tissues/cells, carbon rearrangements of metabolites are tracked and fluxes are estimated by optimized fitting of internal fluxes to the measurements of labeling and external fluxes (substrate uptake and biomass production rates). It has been successfully applied in different plant systems to quantify carbon flow through central metabolism (for recent reviews see Allen et al., 2009; Chen and Shachar-Hill, 2012; Kruger et al., 2012; Kruger and Ratcliffe, 2009; Libourel and Shachar-Hill, 2008; Schwender, 2011). However, steady state MFA is limited to metabolic steps and pathways that involve rearrangement of the label (usually carbon). These limitations lead to the need for dynamic metabolic flux analysis.

Dynamic metabolic flux analysis (DMFA) is an MFA method based on transient labeling experiments (for reviews see Noack et al., 2011; Nöh and Wiechert, 2011; Wiechert et al., 2005). It involves tracking the propagation of labeling patterns through a metabolic network and fitting a kinetic model (in which ordinary differential equations are used to represent reaction rates) to the

*Abbreviations:* NDP-sugars, nucleotide-sugars; Api, apiose; Ara, arabinose; Fuc, fucose; Fru, fructose; Gal, galactose; GalA, galacturonic acid; GDP, guanosine diphosphate; Glc, glucose; GlcA, glucuronic acid; Man, mannose; P, phosphate; Rha, Rhamnose; Xyl, xylose; Suc, Sucrose; G(M)1P, glucose(mannose)-1-phosphate; G(M)6P, glucose(Man)-6-phosphate; F6P, fructose-6-phosphate; Gal1P, galactose-1-phosphate

☆Funding for this work was provided by the Great Lakes Bioenergy Research Center (DOE BER Office of Science DE-FC02-07ER64494).

* Corresponding author. Fax: +1 517 353 1926.
*E-mail addresses:* xwchen@msu.edu, wilson.xw.chen@gmail.com (X. Chen).

1096-7176/$ - see front matter © 2013 Elsevier Inc. All rights reserved.
http://dx.doi.org/10.1016/j.ymben.2013.04.006

dynamic labeling measurements obtained from pulse labeling experiments (without chase or washout). It is able to describe metabolic activities of a network *in vivo* and predict the metabolic effects on network fluxes in response to perturbations. Despite its advantages over steady state MFA, DMFA often requires the development of case specific analytical methods for metabolic intermediate measurements as well as the use of mathematical modeling. Computational frameworks for DMFA are emerging and have been demonstrated or applied in different biological systems (Leighty and Antoniewicz, 2011; Nöh et al., 2006; Selivanov et al., 2004, 2006; Young et al., 2008), but none of these frameworks has been implemented as widely applicable software. Due to these difficulties, DMFA in plant research has been mostly performed in small to medium sized metabolic networks that have little or no carbon skeleton rearrangements (Boatright et al., 2004; Colón et al., 2010; Knoke et al., 2009; Matsuda et al., 2003, 2005, 2007; McNeil et al., 2000; Rios-Estepa et al., 2008; Rohwer and Botha, 2001).

Here we have developed a DMFA model to study the regulation of plant cell wall precursor metabolism. We have monitored the time course of $^{13}C$ labeling in cell wall precursors and related sugar phosphates using a liquid chromatography tandem mass spectrometry method that we previously developed (Alonso et al., 2010). We used the DMFA model based on mass action reaction mechanisms to simulate the carbon flow in the cell wall synthesis network. The kinetic parameters of the model were determined using the time course labeling data of the cell wall precursors. The model allowed us to explore key reactions that control carbon flow to cell wall synthesis and predict *in vivo* metabolic regulation that may affect plant cell wall composition.

## 2. Materials and method

### 2.1. Chemicals

UDP-Xyl, UDP-Ara and UDP-GalA were purchased from the Complex Carbohydrate Research Center (University of Georgia). All the other NDP-sugars and hexose phosphates, excluding UDP-Api and UDP-Rha which are not commercially available, were purchased from Sigma. [U-$^{13}C_{Fru}$]Suc and [U-$^{13}C_{Glc}$] were, respectively, purchased from Omicron Biochemicals, Inc and Isotec (Sigma–Aldrich).

### 2.2. Arabidopsis cell culture, sampling and extraction of metabolites

*Arabidopsis thaliana* ecotype Columbia (cell line T87,Jouanneau and Péaud-Lenoël, 1967) were obtained from the Riken BioResource Center. Cell culture and sampling were performed as previously described (Alonso et al., 2010). Briefly, Arabidopsis T87 cells were cultured in a 7 day culture interval under continuous dark conditions at 22 °C and 120 rpm in a liquid minimal media (Alonso et al., 2010). T87 cells at log phase were centrifuged at 2000 rpm for 3 min at 22 °C. Supernatant was removed under sterile conditions. Cells were transferred to the fresh minimal media containing 100% $^{13}C$ labeled sucrose ([U-$^{13}C_{glc}$]-sucrose or [U-$^{13}C_{fru}$]-sucrose). Cells from 1 mL suspension culture were sampled by fast filtration *via* a nylon membrane filter (Whatman, 0.45 μm pore size and 47 mm diameter) and frozen in liquid nitrogen. Intracellular metabolites were extracted using boiling water (Alonso et al., 2010). The time course of $^{13}C$ labeling in cell wall precursors and related sugar phosphates were monitored using a liquid chromatography tandem mass spectrometry method (Alonso et al., 2010) until isotopic steady state was reached (Supplementary materials Tables S3 and S4). To measure cellular sucrose, fructose and glucose concentration, 3 mL cell suspension was filtered through the membrane filter and the filtrates on the membrane were washed with 6 mL media lacking sucrose. Cellular sugars were measured using Megazyme® sucrose/fructose/D-glucose kits.

### 2.3. External flux measurements

T87 cell growth was measured by monitoring the $OD_{600\ nm}$. Cell suspension was collected at different time points. Cells and cultured medium were separated by centrifugation at 13,000 rpm for 5 min

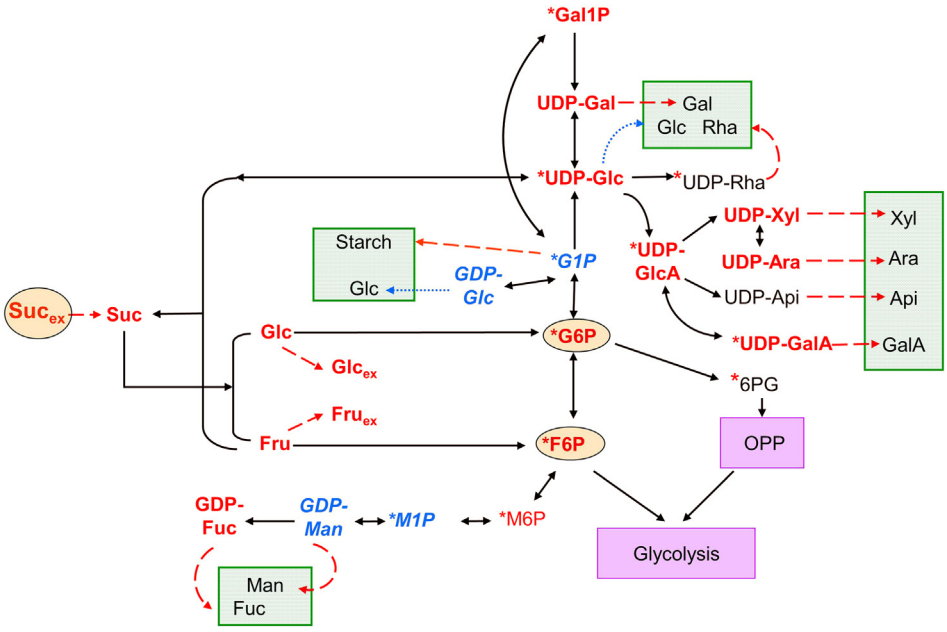


**Fig. 1.** Metabolic network model of plant cell wall synthesis. Bold font (dash line) represents concentration (flux) measurements were made. Star represents labeling measurements were made. Italic font represents concentration measurements that include indistinguishable quantities (GDP-Man and GDP-Glc; and M1P and G1P) and were measured as GDP-HEX and H1P, Dot line represents flux measurements that include indistinguishable quantities (GDP-Glc -> Glc and UDP-Glc -> Glc). Total glucose monomer content in cell wall was used to obtain the sum of two effluxes that depose glucose into cell wall. Circle represents the measured labeling was treated as inputs to the model. Boxes represents terminal of carbon flow.

at 4 °C. Cells were washed with deionized water twice and lyophilized. Glycosyl composition analysis of cell wall was performed at the Complex Carbohydrate Research Center by combined gas chromatography/mass spectrometry of the per-*O*-trimethylsilyl derivatives. Starch measurements were performed as previously described (Alonso et al., 2007), with lipid extraction, followed by washing with 1 mL 80% ethanol twice and starch extraction, hydrolysis and enzyme-based glucose measurement. The starch concentration in cell debris was measured using the Megazyme® Starch Kit. Extracellular uptake rates and production secretion rates were calculated using the equation (Sauer et al., 1999): $v=\left((C(t_2)-C(t_1))/(OD(t_2)-OD(t_1))\cdot f\right)\mu$, where C($t$) and OD($t$) are the extra-cellular metabolite concentrations and $OD_{600}$ at time $t$; $\mu$ is the growth rate of the culture; and $f$ is the conversion coefficient between $OD_{600}$ and biomass dry weight per unit volume of media.

**Table 1**
Growth rate, external flux and intracellular metabolite measurement.

| | |
|---|---|
| $\mu$ (1/day) | 0.41 ± 0.04 |
| $f$ (g dry weight/od/l) | 2.97 ± 0.62 |
| Cell wall/ Cell biomass dry weight | 18% ± 1% |
| $C_{sucrose}$ (nmol/mg dry weight) | 232.4 ± 30.3 |
| $C_{glucose}$ (nmol/mg dry weight) | 50.5 ± 10.1 |
| $C_{fructose}$ (nmol/mg dry weight) | 9.1 ± 5.1 |
| $V_{Suc\_ex}$ (nmol/mg dry weight/day) | 2561.4 ± 102.3 |
| $V_{Glc\_ex}$ (nmol/mg dry weight/day) | 445.3 ± 168.7 |
| $V_{starch}$ (nmol/mg dry weight/day) | 1.0 ± 0.4 |
| $V_{Rha}$ (nmol/mg dry weight/day) | 21.8 ± 2.0 |
| $V_{Fuc}$ (nmol/mg dry weight/day) | 4.1 ± 1.3 |
| $V_{Ara}$ (nmol/mg dry weight/day) | 57.3 ± 3.9 |
| $V_{Xyl}$ (nmol/mg dry weight/day) | 21.9 ± 0.5 |
| $V_{Man}$ (nmol/mg dry weight/day) | 9.1 ± 1.1 |
| $V_{Gal}$ (nmol/mg dry weight/day) | 49.8 ± 2.1 |
| $V_{Glc}$ (nmol/mg dry weight/day) | 208.1 ± 12.3 |
| $V_{Rib}$ (nmol/mg dry weight/day) | 10.5 ± 0.3 |
| $V_{GlcA}$ (nmol/mg dry weight/day) | 0.7 ± 0.3 |
| $V_{GalA}$ (nmol/mg dry weight/day) | 71.7 ± 14.0 |
| $V_{Glc}$ (nmol/mg dry weight/day) | 208.1 ± 12.3 |

### 2.4. Metabolic network model of plant cell wall precursors

A metabolic network of plant cell wall precursors were constructed based on previous pathway studies (Alonso et al., 2010; Reiter, 2008; Seifert, 2004; Sharples and Fry, 2007) (Fig. 1). We developed a DMFA model based on the mass balance principle to simulate the flow of carbon cumomers in the network: $d(m_k^i \cdot C_i)/dt = \sum R_j^{m_k}$, where $C_i$ is the concentration of the precursor $i$, $m_k^i$ is the cumomer $m_k$ of precursor $i$, and $R_j^{m_k}$ is the flux of the reaction $j$ that consumes or produces precursor $i$ with cumomer $m_k$ ($k$=0,3,6). Here mass action kinetics were used to simulate fluxes through each reaction in the network. For example, the balance of carbon cumomer for Gal1P during dynamic labeling experiments (pulse labeling without a chase or washout) can be written as:

$$\frac{d(C_{Gal1P}\cdot m^i_{Gal1P})}{dt} = -V_{Gal1P_{UGal}}\cdot m^i_{Gal1P} - V_{Gal1P_{G1P}}\cdot m^i_{Gal1P} + V_{G1P_{Gal1P}}\cdot m^i_{G1P} \quad (1)$$

The rate equations were listed in Table 1.

The DMFA model was simulated using the PottersWheel software package (Maiwald and Timmer, 2008). The model was simulated in the form of customized ordinary differential equations in the software. In addition to the equation system, two types of constraints were used in the simulation: (1) no change in the pool size of internal metabolites during the dynamic labeling experiments $dC_i/dt = \sum R_j = 0$. This ensures the mass balance of the model in each time step of the parameter fitting; and (2) the ratio of carbon flow into pentose phosphate pathway and glycolysis pathway was constrained to be greater than 39% and less than 65% based on the previous $^{13}C$ metabolic flux analysis of heterotrophic Arabidopsis cell central metabolism (Masakapalli et al., 2010; Williams et al., 2008).

Simulation were performed in a Dell Studio XPS 9100 PC (8 Intel® Core™ CPU at 2.8 GHz, 8.0 GB RAM and 64-bit operating system). Starting from a set of initial parameters, the PottersWheel software gradually adapted the parameter in the ODEs to fit the

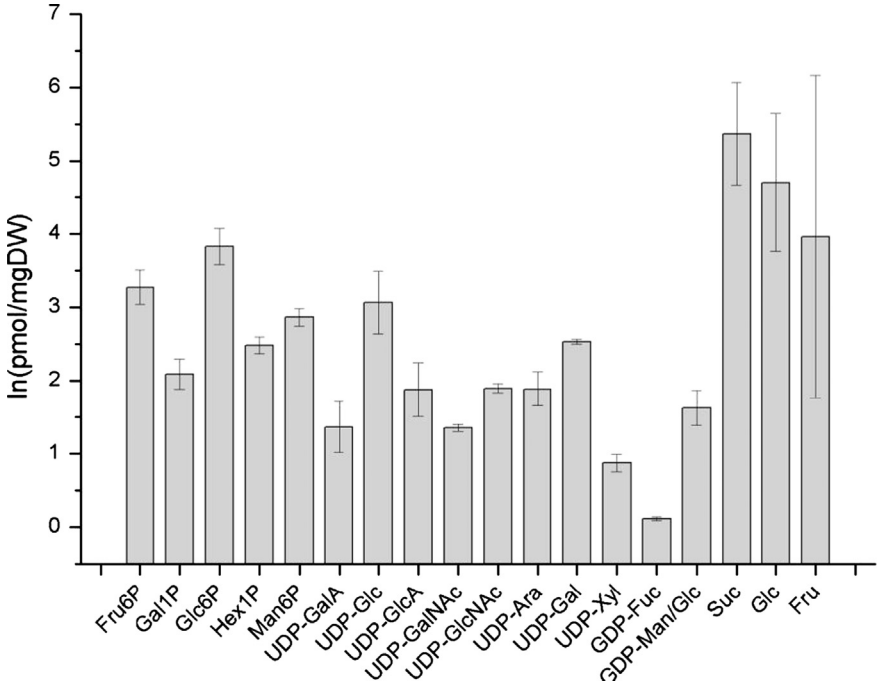


**Fig. 2.** Intracellular metabolite levels. The concentrations of phosphate sugars and nucleotide sugars were obtained from Alonso et al. (2010). Cellular sucrose, glucose and fructose measurements were performed in this work.

labeling, concentration and flux measurements (minimizing the sum of squared residuals weighted by the standard deviation of each measurement ($SS_{res}$)). 320 sets of initial parameter values were used here to avoid finding only local minima. The fittings were performed with disturbed initial parameter values using Trust Region Algorithm in log space. The best fitting result was used to provide the optimized rate constants.

The confidence intervals of the optimized rate constants were estimated using a Monte Carlo approach (Antoniewicz et al., 2006; Libourel and Shachar-Hill, 2008). Fifty datasets were generated using normal distributions $N(\mu, \sigma)$ for each measured quantity, where $\mu$ is the mean of the labeling, concentration or flux measurement and $\sigma$ is the standard deviation of the measurement. The generated data form 50 sets of Monte Carlo pseudo-measurements representing random variations of the original measurements. The DMFA model was fitted to these pseudo-datasets as described in the previous section (104 initial parameter sets were used for each set). The confidence limits were given by the standard deviation of the best fit optimized parameters for each of the 50 pseudo-datasets.

Metabolic control analysis was performed using the software package COPASI 4.7 (Build 34) (Mendes et al., 2009).

## 3. Results and discussion

### 3.1. Model development

Fig. 1 shows the literature derived network (Alonso et al., 2010; Reiter, 2008; Seifert, 2004; Sharples and Fry, 2007) through which carbon flow from the substrate sucrose to cell wall precursors, the oxidative pentose phosphate pathway (OPPP) and glycolysis, and the flow from precursors into cell wall components. The formation of cell wall polymers was assumed to be terminal in the current model. Thus the assembly, modifications and any turnover of cell wall components after monomer polymerization were not considered here. The OPPP and glycolysis pathway were treated as net sinks for carbon flow.

The entry of label into both central metabolism and cell wall precursor pools, originated from the feeding $^{13}C$ labeled sucrose. However since there are reversible reactions in central metabolism, the cell wall network also received $^{13}C$ labeling from central metabolism *via* the common metabolite pools (glucose-6-phosphate (G6P) and fructose-6-phosphate (F6P)) shared by central metabolism and the cell wall synthesis network. We therefore used sucrose, G6P and F6P as labeling input points to the cell wall network in our modeling.

Fig. 1 also summarizes the concentration, labeling and fluxes measurements that we conducted. We measured the concentration of 19 metabolites in the network and time course $^{13}C$ labeling of 10 metabolites (M0, M3 and M6) in the network (Supplementary materials). We were not able to separately measure levels or labeling in two isomeric pairs of metabolites (Man1P and Glc1P; and GDP-Man and GDP-Glc). The two metabolites were modeled separately, and the predicted average labeling was used to match the measurements during fitting.

### 3.2. Fitting and simulation results

320 sets of initial parameter values (rate constants and metabolites) were used here to obtain the global best fitting. The distribution of $SS_{res}$ from 320 fittings was shown in Fig. 4B. The global $SS_{res}/N$ is 64.3 m, where $N$ is the number of measurements used in the fitting ($N=361$). The optimized parameter values and their confidence interval in the form of standard deviations are shown in Table 2 and Supplemental materials Table S1. The mean of best fit parameters from Monte Carlo simulation were shown in Supplemental materials Tables S1 and S2. Overall, 56% of the normalized (to the mean of optimized kinetic constants) standard deviation is smaller than 0.3. For the normalized standard deviations that were greater than 30%, 35% of

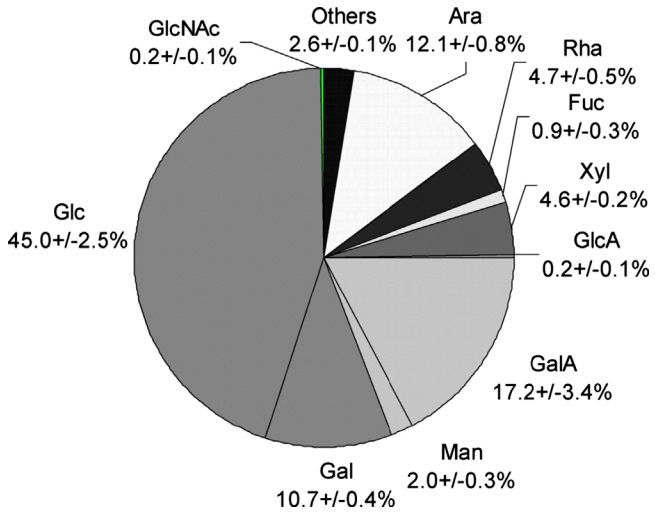


**Fig. 3.** Cell wall glycosyl composition (grams glycosyl residue/100 g biomass dry weight).

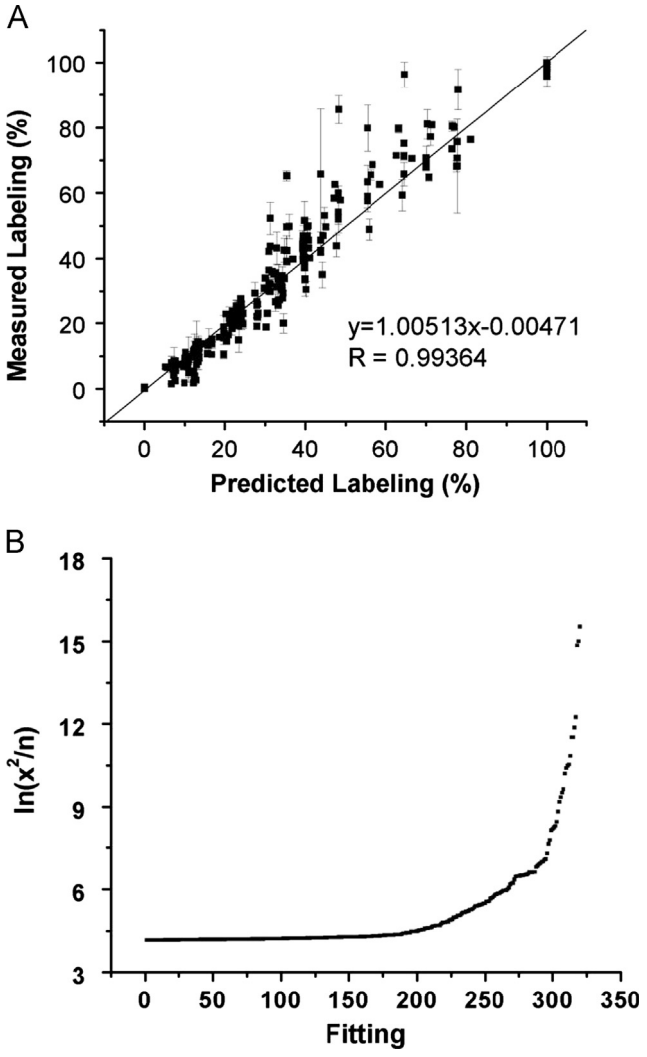


**Fig. 4.** (A) Correlation plot between measurement and prediction; and (B) fitting residues from 320 fittings.

**Table 2**
Rate equation and optimized rate constant.

| | Flux Name | Direction | Reaction | Rate equation | Rate constant ($k$) | std |
|---|---|---|---|---|---|---|
| 1 | $V_{uptake}$ | | $Suc_{ex} \rightarrow Suc_{Cellular}$ | K | 2.56E+03 | 9.85E+1 |
| 2 | $V_{suc\ synthase}^{+}$ | → | Suc⇔UDP-Glc+Fru | $K^*C_{Suc}$ | 1.80E−02 | 5.57E−03 |
| | $V_{suc\ synthase}^{-}$ | ← | | $K^*C_{UDP\text{-}Glc}{}^*C_{Fru}$ | 1.52E−05 | 2.04E−03 |
| 3 | $V_{suc\ invertase}$ | | Suc→Glc+Fru | $K^*C_{suc}$ | 1.13E+01 | 4.38E−01 |
| 4 | $V_{F6P\text{-}M6P}$ | → | F6P⇔M6P | $K^*C_{F6P}$ | 8.93E+00 | 7.42E−01 |
| | $V_{M6P\text{-}F6P}$ | ← | | $K^*C_{M6P}$ | 9.65E−01 | 5.43E−01 |
| 5 | $V_{M6P\text{-}M1P}$ | → | M6P⇔M1P | $K^*C_{M6P}$ | 1.83E+01 | 1.48E+00 |
| | $V_{M1P\text{-}M6P}$ | ← | | $K^*C_{M1P}$ | 5.01E−01 | 1.57E+00 |
| 6 | $V_{M1P\text{-}GMan}$ | → | M1P→GDP-Man | $K^*C_{M1P}$ | 7.48E+01 | 1.76E+01 |
| | $V_{GMan\text{-}M1P}$ | ← | | $K^*C_{GDP\text{-}Man}$ | 1.30E+01 | 7.77E+01 |
| 7 | $V_{efflux\text{-}Man}$ | | GDP-Man→ | $K^*C_{GDP\text{-}Man}$ | 3.33E+02 | 4.37E+01 |
| 8 | $V_{efflux\text{-}Fuc}$ | | GDP-Man→ | $K^*C_{GDP\text{-}Man}$ | 1.26E+02 | 2.16E+01 |
| 9 | $V_{Gal1P\text{-}UGal}$ | | Gal1P→UDP-Gal | $K^*C_{Gal1P}$ | 6.97E−01 | 1.31E+00 |
| 10 | $V_{Gal1P\text{-}G1P}$ | → | Gal1P⇔G1P | $K^*C_{Gal1P}$ | 5.33E−02 | 2.18E−01 |
| | $V_{G1P\text{-}Gal1P}$ | ← | | $K^*C_{G1P}$ | 5.37E−01 | 9.42E−01 |
| 11 | $V_{UGal\text{-}UGlc}$ | → | UDP-Gal⇔UDP-Glc | $K^*C_{UDP\text{-}Gal}$ | 1.69E+00 | 1.61E+00 |
| | $V_{UGlc\text{-}UGal}$ | ← | | $K^*C_{UDP\text{-}Glc}$ | 3.41E+01 | 1.41E+00 |
| 12 | $V_{G1P\text{-}UGlc}$ | | G1P→UDP-Glc | $K^*C_{G1P}$ | 2.97E+03 | 9.67E+02 |
| 13 | $V_{G1P\text{-}G6P}$ | → | G1P⇔G6P | $K^*C_{G1P}$ | 6.17E+00 | 1.00E+01 |
| | $V_{G6P\text{-}G1P}$ | ← | | $K^*C_{G6P}$ | 6.36E+01 | 3.03E+00 |
| 14 | $V_{UGlc\text{-}URha}$ | | UDP-Glc→UDP-Rha | $K^*C_{UDP\text{-}Glc}$ | 1.11E+01 | 1.73E+00 |
| 15 | $V_{UGlc\text{-}UGlcA}$ | | UDP-Glc→UDP-GlcA | $K^*C_{UDP\text{-}Glc}$ | 9.82E+01 | 9.32E+00 |
| 16 | $V_{UGlcA\text{-}UGalA}$ | → | UDP-GlcA⇔UDP-GalA | $K^*C_{UDP\text{-}GlcA}$ | 6.77E+02 | 1.23E+02 |
| | $V_{UGalA\text{-}UGlcA}$ | ← | | $K^*C_{UDP\text{-}GalA}$ | 3.10E+01 | 1.18E+01 |
| 17 | $V_{G6P\text{-}6PG}$ | | G6P→6PG | $K^*C_{G6P}$ | 2.68E+02 | 2.70E+01 |
| 18 | $V_{efflux\text{-}Gal}$ | | UDP-Gal→ | $K^*C_{UDP\text{-}Gal}$ | 1.47E+02 | 5.76E+00 |
| 19 | $V_{efflux\text{-}Glc1}$ | | UDP-Glc→ | $K^*C_{UDP\text{-}Glc}$ | 1.40E+02 | 8.44E+00 |
| 20 | $V_{G1P\text{-}GGlc}$ | → | G1P⇔GDP-Glc | $K^*C_{G1P}$ | 3.44E+00 | 3.38E+00 |
| | $V_{GGlc\text{-}G1P}$ | ← | | $K^*C_{GDP\text{-}Gld}$ | 5.98E+01 | 3.90E+01 |
| 21 | $V_{efflux\_Glc2}$ | | GDP-Glc→ | $K^*C_{GDP\text{-}Glc}$ | 4.51E-01 | 1.16E+01 |
| 22 | $V_{efflux\_Rha}$ | | UDP-Rha→ | $K^*C_{UDP\text{-}Rha}$ | 1.64E+01 | 2.56E+00 |
| 23 | $V_{efflux\_xyl}$ | | UDP-GlcA→ | $K^*C_{UDP\text{-}GlcA}$ | 2.22E+02 | 1.81E+01 |
| 24 | $V_{efflux\_Ara}$ | | UDP-GlcA→ | $K^*C_{UDP\text{-}GlcA}$ | 4.63E+02 | 5.54E+01 |
| 25 | $V_{efflux\_GalA}$ | | UDP-GalA→ | $K^*C_{UDP\text{-}GalA}$ | 2.68E+03 | 4.96E+02 |
| 26 | $V_{efflux\_OPPP}$ | | 6PG→ | $K^*C_{6PG}$ | 1.57E+06 | 1.58E+05 |
| 27 | $V_{efflux\_ex\_Glc}$ | | Glc→ | $K^*C_{Glc}$ | 4.02E+00 | 1.74E+00 |
| 28 | $V_{efflux\_starch}$ | | G1P→ | $K^*C_{G1P}$ | 7.42E+00 | 2.92E+00 |
| 29 | $V_{Fru\text{-}F6P}$ | | Fru→F6P | $K^*C_{Fru}$ | 3.07E+02 | 1.18E+01 |
| 30 | $V_{Glc\text{-}G6P}$ | | Glc→G6P | $K^*C_{Glc}$ | 4.91E+01 | 2.77E+00 |

them came from reactions with small fluxes. A correlation plot of the measurement constraints used in fitting and model predicted results is shown in Fig. 4A. The labeling prediction for several metabolites during the dynamic labeling experiments was shown in Fig. 5.

### 3.3. Physiology

Figs. 2 and 3, and Table 1 depict the physiology of T87 cells in the culture conditions used. The cells were maintained in metabolic steady state (the pool sizes of metabolic intermediates remained the same through the time course) during the dynamic labeling experiments. T87 cells grew in the current culture condition at a growth rate of $0.41 \pm 0.04\ day^{-1}$. The glycosyl components in the cell wall accounted for 18% ±1% of total biomass dry weight. This corresponds to a significant portion of carbon uptake being incorporated into the cell walls (~8.8%). This is in the range of previous findings in Arabidopsis cell culture (Masakapalli et al., 2010; Williams et al., 2008).

### 3.4. Flux map

The flux map of cell wall synthesis network at metabolic steady state is shown in Fig. 6. The results describe the routes and rates of carbon flow from sucrose to cell wall precursors. We found that sucrose invertase is responsible for the entry of sucrose into metabolism in T87 cells. More than 99% of carbon entered cellular metabolism *via* sucrose invertase under these growth conditions. The carbon flow was then directed to cell wall precursor synthesis through phosphoglucomutase and phosphomannose isomerase.

Our results provide evidence on the role of sucrose invertase in cellulose and starch production, which has been a topic of debate in recent years (Baroja-Fernández et al., 2012; Barratt et al., 2009; Bieniawska et al., 2007). Barratt et al. (2009) generated Arabidopsis mutant plants that lack isoforms of sucrose invertase and sucrose synthase, respectively. It was found that the plants that lack sucrose synthase activities had normal growth phenotypes, but the sucrose invertase mutant plants had severely reduced growth rates. Baroha-Fernandez et al. used a different method to assay sucrose synthase activity in plant extracts and reported that the activities can support normal starch and cellulose biosynthesis. Their work, however, did not assay the activities of sucrose invertase in the same plant extracts. Our results provided evidence that *in vivo* invertase activity carries about over 99% of the entry of sucrose into metabolism. This supports an important role for sucrose invertase in the entry of sucrose into metabolism in heterotrophic cells under aerobic conditions. Our results suggested that phosphoglucomutase (Glc6P→Glc1P) may act as a critical step that directs carbon flow to cell wall synthesis.

Our flux map shows that UDP-Glc-4-epimerase plays a dominant role in UDP-Gal synthesis in heterotrophic Arabidopsis cells culture. UDP-Gal can be synthesized *via* unidirectional UDP-Gal pyrophosphorylase and bidirectional UDP-Glc-4-epimerase in plants. Sharples and Fry conducted a dual-radiolabeling experiment on Arabidopsis cells cultured in a glycerol medium (Sharples and Fry, 2007). The cell culture was fed with traces of D-[1-$^{3}$H] galactose and [U-$^{14}$C] fructose. $^{3}$H:$^{14}$C ratios decreased in the order of Gal1P, UDP-Gal, UDP-Glc, G1P, G6P and F6P. These results

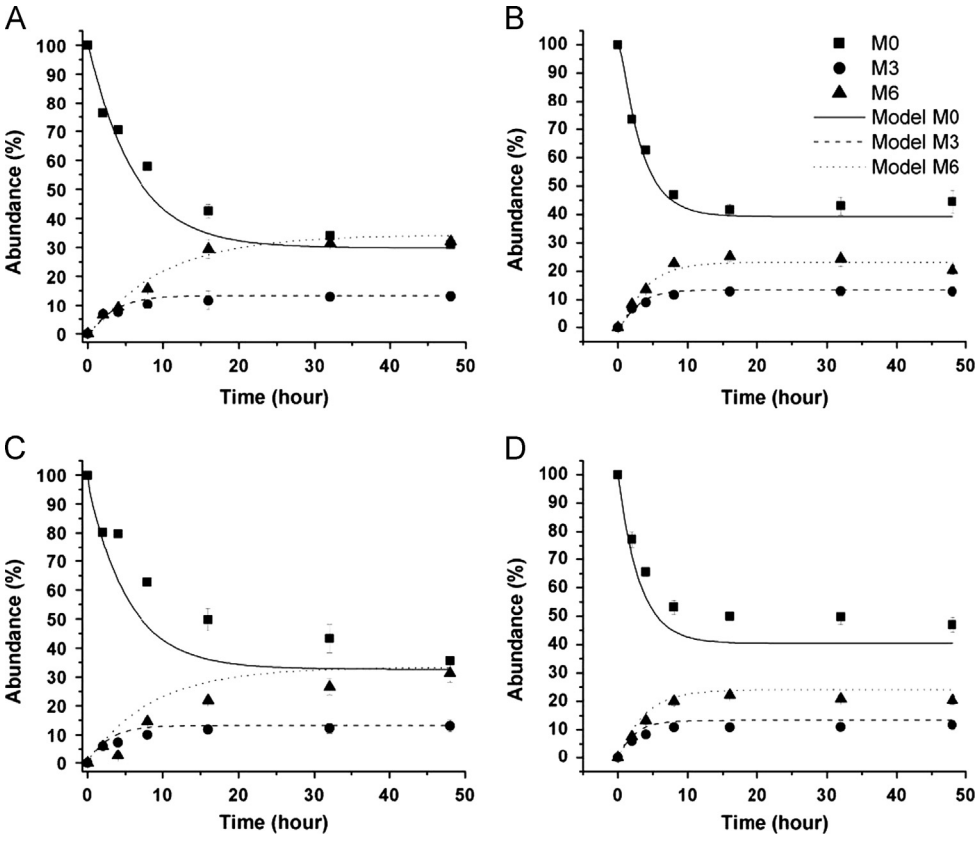


**Fig. 5.** Labeling measurements and model prediction. (A) Gal1P in [U-$^{13}C_{fru}$]-sucrose experiments; (B) Gal1P in [U-$^{13}C_{fru}$]-sucrose experiments; (C) Hex1P in [U-$^{13}C_{fru}$]-sucrose experiments; and D: Hex1P in [U-$^{13}C_{fru}$]-sucrose experiments.

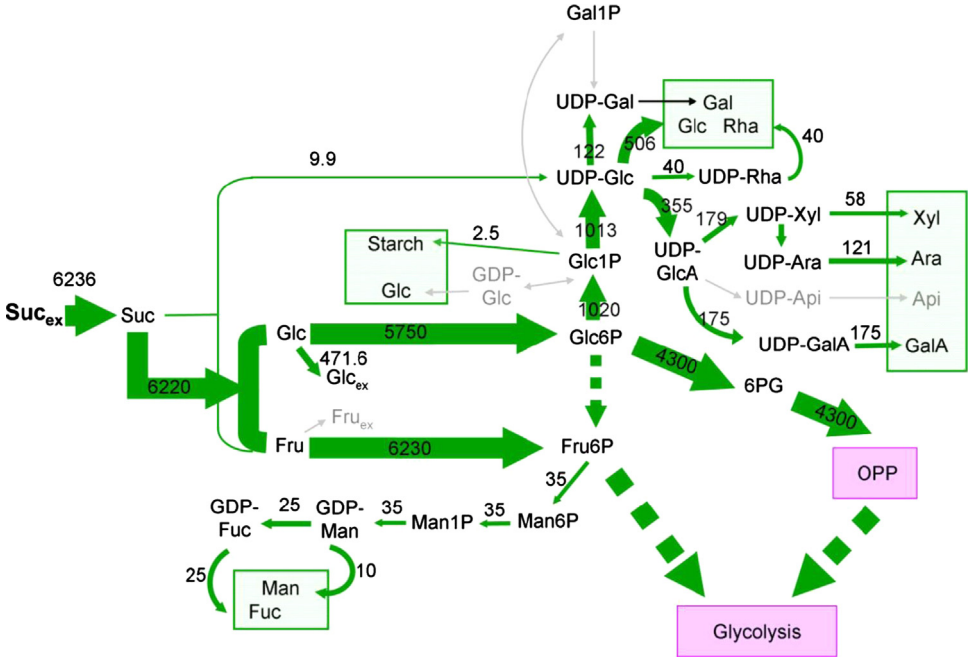


**Fig. 6.** Flux map at metabolic steady state. Flux unit: nmol/mg DW.

demonstrated the existence of both UDP-Gal pyrophosphorylase and UDP-Glc-4-epimerase activities in the Arabidopsis cell culture. The relative importance of the two enzymes in UDP-Gal synthesis was not determined in that work. Our results show that UDP-Gal is almost solely synthesized from UDP-Glc *via* UDP-Glc-4-epimerase. This finding is also consistent with previous reverse genetic studies. Rösti et al. (2007) studied *A. thaliana* mutant plants and found that UDP-Glc-4-epimerase isoforms cooperate in providing UDP-Gal for cell wall biosynthesis and growth of *A. thaliana* . The dominant role of UDP-Glc-4-epimerase over UDP-Gal pyrophosphorylase suggests that the former enzyme may be a more promising target for designing biofuel crops.

We considered whether inaccuracies in pool sizes might affect the flux map and found that the fluxes derived from the modeling

**Table 3**
Reactions that may affect carbon flow to cell wall xylose.

| Reaction | Flux control coefficient(%) |
|---|---|
| Glc6P→Glc1P | 99 |
| UDP-Glc→UDP-GlcA | 65 |
| UDP-GlcA→UDP-GalA | −49 |
| UDP-Glc→cell wall Glc | −50 |
| UDP-Ara→cell wall Ara | −34 |

are independent of the pool sizes used. This can be shown both theoretically and empirically. Theoretically, each flux of material (reaction rate) is modeled as the product of a substrate concentration and a rate constant, and each flux of label (rate of 13C flow) is modeled as the product of the product of the same substrate concentration and rate constant multiplied by the labeling level of the substrate. Therefore the value of a metabolite concentration always appears multiplied by the relevant rate constant. Therefore if a metabolite concentration was incorrect because of compartmentation, modeling with a corrected concentration would result in the value of the rate constant obtained from the model being changed by the inverse of the same factor, leaving the flux unchanged. Empirically, we confirmed this by arbitrarily changing several of the concentrations used in the modeling and observing that the change of the flux values obtained are all within the confidence intervals calculated from the Monte Carlo approach (less than 1.9% of total carbon uptake rates) although the rate constants were different as predicted.

### 3.5. Predictions

One important goal of this study was to understand the regulation of cell wall synthesis network aid the design of plants with improved cell wall compositions. Here we performed metabolic control analysis to obtain insights into the regulation of cell wall precursor synthesis (Burns et al., 1985; Fell, 1992, 1997). The resulting flux control coefficients (Supplementary materials Table S5) depict how modest perturbations of enzyme activities can affect metabolic fluxes in the cell wall synthesis network.

Pentose sugar contents such as xylose in plant cell wall are difficult to ferment by microbes, therefore representing an important target for metabolic engineering of bioenergy crops. Table 3 highlighted the perturbations that may significantly affect carbon flow to cell wall xylose synthesis. The results show that doubling the expression of phosphoglucomutase and UDP-Glc dehydrogenase (UDP-Glc→UDP-GlcA) may increase the carbon flux to cell wall xylose by 99% and 65%, respectively, and doubling the expression of UDP-GlcA-4-epimerase (UDP-GlcA→UDP-GalA) and enzymes for cell wall glucose (UDP-Glc→cell wall Glc) and cell wall arabinose (UDP-Ara→cell wall Ara) synthesis may reduce cell wall xylose formation significantly. Interestingly, the perturbations of enzymes that are adjacent to carbon entry (sucrose invertase) have stronger impacts on the cell wall xylose formation fluxes.

### 3.6. Limitations

The mathematical model developed here is presented as a tool for exploring the kinetic regulation of plant cell wall synthesis *in vivo*. The model was able to explain the time course data for multiple isotopically labeled forms (mass isotopomers) of multiple metabolites in terms of pathway delineation and prediction of metabolic regulation under steady state growth. However significant simplifications were made in the current approach.

The network was modeled as a one-compartment system while some metabolites such as G6P and F6P appear in both cytosol and plastid. This was done because we were not able to reliably quantify levels or labeling of the same metabolite in different subcellular compartments. Steady state MFA studies have used compartment-specific products (Allen et al., 2007) to measure the labeling of sugar phosphate and nucleotide sugars in the cytosol and chloroplast (Lonien and Schwender, 2009; Masakapalli et al., 2010; Williams et al., 2008). However steady state labeling patterns cannot reliably predict potential compartmental differences during dynamic labeling. To overcome this challenge and refine the model it may be feasible to use non-aqueous fractionation (Farré et al., 2001; Krueger et al., 2011) to isolate and analyze pools from cytosol and plastid.

The kinetics were modeled as linear mass action rates for each reaction in the network. This simplification is because the dynamic labeling experiments were performed at metabolic steady state, therefore the labeling data cannot determine the non-linear enzymatic behavior or catalytic effects due to inhibitor/activator/allosteric regulators. This approach is usual among dynamic labeling studies of networks of moderate or larger size (Libourel and Shachar-Hill, 2008).

To relieve these limitations, methods for quantifying metabolites and cosubstrates at the subcellular compartment level need to be further developed (especially for labile metabolic intermediates), and metabolomic profiling experiments at metabolic non-steady state will need to be conducted.

## 4. Conclusion

We have developed a kinetic model based on mass action reaction mechanisms to simulate the carbon flow in the cell wall synthesis network. We have determined the kinetic parameters of the model using the time course labeling data of the intermediates within the metabolic network. The results revealed sucrose invertase as the primary entering point of carbon into metabolism under non-photosynthetic cell suspension culture condition, and suggested that phosphoglucomutase (Glc6P→Glc1P) may have a significant regulatory role in carbon flow to cell wall synthesis. The computational modeling also predicted *in vivo* metabolic regulation that may affect plant cell wall composition.

## Acknowledgment

The authors would like to thank Drs. Dan Jones and Lijun Chen (MSU Mass Spectrometry Facility) for expert help with instrumental analyses; Dr. Hart Poskar for his effort on developing previous versions of the model; Tina M. Martin, Rebecca J. Piasecki and Russell W. LaClair for their technical support in cell cultures, enzyme assays and LC-MS/MS analyses; We are also grateful to Dr. Thomas Maiwald for his assistance on PottersWheel. The Glycosyl composition analysis was performed at the DOE-funded (DE-FG02-09ER-20097) Center for Plant and Microbial Complex Carbohydrates. This work was supported by the Great Lakes Bioenergy Research Center (DOE BER Office of Science DE-FC02-07ER64494).

## Appendix A. Supporting information

Supplementary data associated with this article can be found in the online version at http://dx.doi.org/10.1016/j.ymben.2013.04.006.

## References

Allen, D.K., Libourel, I.G., Shachar-Hill, Y., 2009. Metabolic flux analysis in plants: coping with complexity. Plant Cell Environ. 32, 1241–1257.

Allen, D.K., Shachar-Hill, Y., Ohlrogge, J.B., 2007. Compartment-specific labeling information in $^{13}C$ metabolic flux analysis of plants. Phytochemistry 68, 2197–2210.
Alonso, A.P., Piasecki, R.J., Wang, Y., LaClair, R.W., Shachar-Hill, Y., 2010. Quantifying the labeling and the levels of plant cell wall precursors using ion chromatography tandem mass spectrometry. Plant Physiol. 153, 915–924.
Alonso, A.P., Raymond, P., Hernould, M., Rondeau-Mouro, C., de Graaf, A., Chourey, P., Lahaye, M., Shachar-Hill, Y., Rolin, D., Dieuaide-Noubhani, M., 2007. A metabolic flux analysis to study the role of sucrose synthase in the regulation of the carbon partitioning in central metabolism in maize root tips. Metab. Eng. 9, 419–432.
Antoniewicz, M.R., Kelleher, J.K., Stephanopoulos, G., 2006. Determination of confidence intervals of metabolic fluxes estimated from stable isotope measurements. Metab. Eng. 8, 324–337.
Antoniewicz, M.R., Kelleher, J.K., Stephanopoulos, G., 2007. Elementary metabolite units (EMU): a novel framework for modeling isotopic distributions. Metab. Eng. 9, 68–86.
Bar-Peled, M., O'Neill, M.A., 2011. Plant Nucleotide Sugar Formation, Interconversion, and Salvage by Sugar Recycling*. Annu. Rev. Plant Biol. 62, 127–155.
Baroja-Fernández, E., Muñoz, F.J., Li, J., Bahaji, A., Almagro, G., Montero, M., Etxeberria, E., Hidalgo, M., Sesma, M.T., Pozueta-Romero, J., 2012. Sucrose synthase activity in the sus1/sus2/sus3/sus4 Arabidopsis mutant is sufficient to support normal cellulose and starch production. Proc. Natl. Acad. Sci. U. S. A. 109, 321–326.
Barratt, D.H., Derbyshire, P., Findlay, K., Pike, M., Wellner, N., Lunn, J., Feil, R., Simpson, C., Maule, A.J., Smith, A.M., 2009. Normal growth of Arabidopsis requires cytosolic invertase but not sucrose synthase. Proc. Natl. Acad. Sci. U. S. A. 106, 13124–13129.
Bieniawska, Z., Paul Barratt, D.H., Garlick, A.P., Thole, V., Kruger, N.J., Martin, C., Zrenner, R., Smith, A.M., 2007. Analysis of the sucrose synthase gene family in Arabidopsis. Plant J. 49, 810–828.
Boatright, J., Negre, F., Chen, X., Kish, C.M., Wood, B., Peel, G., Orlova, I., Gang, D., Rhodes, D., Dudareva, N., 2004. Understanding *in vivo* benzenoid metabolism in petunia petal tissue. Plant Physiol. 135, 1993–2011.
Burns, J.A., Cornish-Bowden, A., Groen, A.K., Heinrich, R., Kacser, H., Porteous, J.W., Rapoport, S.M., Rapoport, T.A., Stucki, J.W., Tager, J.M., 1985. Control analysis of metabolic systems. Trends Biochem. Sci. 10, 16 16.
Carpita, N.C., 2012. Progress in the biological synthesis of the plant cell wall: new ideas for improving biomass for bioenergy. Curr. Opin. Biotechnol. 23, 330–337.
Chen, X., Shachar-Hill, Y., 2012. Insights into metabolic efficiency from flux analysis. J. Exp. Bot. 63, 2343–2351.
Chundawat, S.P.S., Beckham, G.T., Himmel, M.E., Dale, B.E., 2011. Deconstruction of lignocellulosic biomass to fuels and chemicals. Annu. Rev. Chem. Biomol. Eng. 2 (121-145).
Colón, A.M., Sengupta, N., Rhodes, D., Dudareva, N., Morgan, J., 2010. A kinetic model describes metabolic response to perturbations and distribution of flux control in the benzenoid network of Petunia hybrida. Plant J. 62, 64–76.
Farré, E.M., Tiessen, A., Roessner, U., Geigenberger, P., Trethewey, R.N., Willmitzer, L., 2001. Analysis of the compartmentation of glycolytic intermediates, nucleotides, sugars, organic acids, amino acids, and sugar alcohols in potato tubers using a nonaqueous fractionation method. Plant Physiol. 127, 685–700.
Fell, D., 1997. Understanding the Control of Metabolism. Portland Press Ltd, London.
Fell, D.A., 1992. Metabolic control analysis: a survey of its theoretical and experimental development. Biochem. J. 286, 313–330.
Jouanneau, J.P., Péaud-Lenoël, C., 1967. Growth and synthesis of proteins in cell suspensions of a kinetin dependent tobacco. Physiol. Plant 20, 834–850.
Keegstra, K., Cavalier, D., 2011. Glycosyltransferases of the GT34 and GT37 Families. Annu. Plant Rev. 41, 235–249.
Knoke, B., Textor, S., Gershenzon, J., Schuster, S., 2009. Mathematical modelling of aliphatic glucosinolate chain length distribution in *Arabidopsis thaliana* leaves. Phytochem. Rev. 8, 39–51.
Krueger, S., Giavalisco, P., Krall, L., Steinhauser, M.C., Büssis, D., Usadel, B., Flügge, U. I., Fernie, A.R., Willmitzer, L., Steinhauser, D., 2011. A topological map of the compartmentalized *Arabidopsis thaliana* leaf metabolome. PLoS One 6, e17806.
Kruger, N.J., Masakapalli, S.K., Ratcliffe, R.G., 2012. Strategies for investigating the plant metabolic network with steady-state metabolic flux analysis: lessons from an Arabidopsis cell culture and other systems. J. Exp. Bot. 63, 2309–2323.
Kruger, N.J., Ratcliffe, R.G., 2009. Insights into plant metabolic networks from steady-state metabolic flux analysis. Biochimie 91, 697–702.
Leighty, R.W., Antoniewicz, M.R., 2011. Dynamic metabolic flux analysis (DMFA): a framework for determining fluxes at metabolic non-steady state. Metab. Eng. 13, 745–755.
Libourel, I.G., Shachar-Hill, Y., 2008. Metabolic flux analysis in plants: from intelligent design to rational engineering. Annu. Rev. Plant Biol. 59, 625–650.
Lonien, J., Schwender, J., 2009. Analysis of metabolic flux phenotypes for two Arabidopsis mutants with severe impairment in seed storage lipid synthesis. Plant Physiol. 151, 1617–1634.
Maiwald, T., Timmer, J., 2008. Dynamical modeling and multi-experiment fitting with PottersWheel. Bioinformatics 24, 2037–2043.
Martinez, A.T., Ruiz-Duenas, F.J., Martinez, M.J., Del Rio, J.C., Gutierrez, A., 2009. Enzymatic delignification of plant cell wall: from nature to mill. Curr. Opin. Biotechnol. 20, 348–357.
Masakapalli, S.K., Le Lay, P., Huddleston, J.E., Pollock, N.L., Kruger, N.J., Ratcliffe, R.G., 2010. Subcellular flux analysis of central metabolism in a heterotrophic Arabidopsis cell suspension using steady-state stable isotope labeling. Plant Physiol. 152, 602–619.
Matsuda, F., Morino, K., Ano, R., Kuzawa, M., Wakasa, K., Miyagawa, H., 2005. Metabolic flux analysis of the phenylpropanoid pathway in elicitor-treated potato tuber tissue. Plant Cell Physiol. 46, 454–466.
Matsuda, F., Morino, K., Miyashita, M., Miyagawa, H., 2003. Metabolic flux analysis of the phenylpropanoid pathway in wound-healing potato tuber tissue using stable isotope-labeled tracer and LC-MS spectroscopy. Plant Cell Physiol. 44, 510–517.
Matsuda, F., Wakasa, K., Miyagawa, H., 2007. Metabolic flux analysis in plants using dynamic labeling technique: application to tryptophan biosynthesis in cultured rice cells. Phytochemistry 68, 2290–2301.
McNeil, S.D., Nuccio, M.L., Rhodes, D., Shachar-Hill, Y., Hanson, A.D., 2000. Radiotracer and computer modeling evidence that phospho-base methylation is the main route of choline synthesis in tobacco. Plant Physiol. 123, 371–380.
Mendes, P., Hoops, S., Sahle, S., Gauges, R., Dada, J., Kummer, U., 2009. Computational modeling of biochemical networks using COPASI. Methods Mol. Biol. 500, 17–59.
Nanchen, A., Fuhrer, T., Sauer, U., 2007. Determination of metabolic flux ratios from 13C-experiments and gas chromatography-mass spectrometry data: protocol and principles. Methods Mol. Biol. 358, 177–197.
Noack, S., Nöh, K., Moch, M., Oldiges, M., Wiechert, W., 2011. Stationary versus non-stationary 13C-MFA: A comparison using a consistent dataset. Journal of Biotechnology 154, 179–190.
Nöh, K., Wahl, A., Wiechert, W., 2006. Computational tools for isotopically instationary 13C labeling experiments under metabolic steady state conditions. Metab. Eng. 8, 554–577.
Nöh, K., Wiechert, W., 2011. The benefits of being transient: isotope-based metabolic flux analysis at the short time scale. Appl. Microbiol. Biotechnol. 91, 1247–1265.
Pauly, M., Keegstra, K., 2010. Plant cell wall polymers as precursors for biofuels. Curr. Opin. Plant Biol. 13, 304–311.
Reiter, W.D., 2008. Biochemical genetics of nucleotide sugar interconversion reactions. Curr. Opin. Plant Biol. 11, 236–243.
Rios-Estepa, R., Turner, G.W., Lee, J.M., Croteau, R.B., Lange, B.M., 2008. A systems biology approach identifies the biochemical mechanisms regulating monoterpenoid essential oil composition in peppermint. Proc. Natl. Acad. Sci. U. S. A. 105, 2818–2823.
Rohwer, J.M., Botha, F.C., 2001. Analysis of sucrose accumulation in the sugar cane culm on the basis of in vitro kinetic data. Biochem. J. 358, 437–445.
Rösti, J., Barton, C.J., Albrecht, S., Dupree, P., Pauly, M., Findlay, K., Roberts, K., Seifert, G.J., 2007. UDP-glucose 4-epimerase isoforms UGE2 and UGE4 cooperate in providing UDP-galactose for cell wall biosynthesis and growth of *Arabidopsis thaliana*. Plant Cell. 19, 1565–1579.
Sauer, U., Lasko, D.R., Fiaux, J., Hochuli, M., Glaser, R., Szyperski, T., Wuthrich, K., Bailey, J.E., 1999. Metabolic flux ratio analysis of genetic and environmental modulations of *Escherichia coli* central carbon metabolism. J. Bacteriol. 181, 6679–6688.
Schmidt, K., Carlsen, M., Nielsen, J., Villadsen, J., 1997. Modeling isotopomer distributions in biochemical networks using isotopomer mapping matrices. Biotechnol. Bioeng. 55, 831–840.
Schwender, J., 2011. Experimental flux measurements on a network scale. Front. Plant Sci., 2.
Seifert, G.J., 2004. Nucleotide sugar interconversions and cell wall biosynthesis: how to bring the inside to the outside. Curr. Opin. Plant Biol. 7, 277–284.
Selivanov, V.A., Marin, S., Lee, P.W.N., Cascante, M., 2006. Software for dynamic analysis of tracer-based metabolomic data: estimation of metabolic fluxes and their statistical analysis. Bioinformatics 22, 2806–2812.
Selivanov, V.A., Puigjaner, J., Sillero, A., Centelles, J.J., Ramos-Montoya, A., Lee, P.W. N., Cascante, M., 2004. An optimized algorithm for flux estimation from isotopomer distribution in glucose metabolites. Bioinformatics 20, 3387–3397.
Sharples, S.C., Fry, S.C., 2007. Radioisotope ratios discriminate between competing pathways of cell wall polysaccharide and RNA biosynthesis in living plant cells. Plant J. 52, 252–262.
Somerville, C., Bauer, S., Brininstool, G., Facette, M., Hamann, T., Milne, J., Osborne, E., Paredez, A., Persson, S., Raab, T., Vorwerk, S., Youngs, H., 2004. Toward a systems approach to understanding plant cell walls. Science 306, 2206–2211.
Wiechert, W., de Graaf, A.A., 1997. Bidirectional reaction steps in metabolic networks: I. Modeling and simulation of carbon isotope labeling experiments. Biotechnol. Bioeng. 55, 101–117.
Wiechert, W., Nöh, K., Kragl, U., 2005. From stationary to instationary metabolic flux analysis. Adv. Biochem. Eng. Biotechnol. 92, 145–172.
Wiechert, W., Siefke, C., de Graaf, A.A., Marx, A., 1997. Bidirectional reaction steps in metabolic networks: II. Flux estimation and statistical analysis. Biotechnol. Bioeng. 55, 118–135.
Williams, T.C., Miguet, L., Masakapalli, S.K., Kruger, N.J., Sweetlove, L.J., Ratcliffe, R. G., 2008. Metabolic network fluxes in heterotrophic Arabidopsis cells: stability of the flux distribution under different oxygenation conditions. Plant Physiol. 148, 704–718.
Wittmann, C., 2002. Metabolic flux analysis using mass spectrometry. Adv. Biochem. Eng. Biotechnol. 74, 39–64.
Young, J.D., Walther, J.L., Antoniewicz, M.R., Yoo, H., Stephanopoulos, G., 2008. An elementary metabolite unit (EMU) based method of isotopically nonstationary flux analysis. Biotechnol. Bioeng. 99, 686–699.
Zamboni, N., Fendt, S.M., Ruhl, M., Sauer, U., 2009. 13C-based metabolic flux analysis. Nat. Protoc. 4, 878–892.
Zamboni, N., Fischer, E., Sauer, U., 2005. FiatFlux—a software for metabolic flux analysis from 13C-glucose experiments. BMC Bioinform. 6, 209.
Zhang, B., Liu, X., Qian, Q., Liu, L., Dong, G., Xiong, G., Zeng, D., Zhou, Y., 2011. Golgi nucleotide sugar transporter modulates cell wall biosynthesis and plant growth in rice. Proc. Natl. Acad. Sci. U. S. A. 108, 5110–5115.